Article

Not peer-reviewed version

An influence of fluorinated alkyl substituents on structure and magnetic properties of Mn(II) complexes with pyrazolyl-substituted nitronyl nitroxides

Ekaterina Kudryavtseva , Andrey Serykh , Bogdan Ugrak , Tatyana Dutova , Darina I. Nasyrova , Alexander Korlyukov , Mikhail A. Zykin , Nikolay Nikolaevich Efimov , Artem S. Bogomyakov , Evgeny Tretyakov *

Posted Date: 26 September 2023

doi: 10.20944/preprints202309.1700.v1

Keywords: nitronyl nitroxides; metal-nitroxide complexes; crystal structures; magnetic properties

Article

An Influence of Fluorinated Alkyl Substituents on Structure and Magnetic Properties of Mn(II) Complexes with Pyrazolyl-Substituted Nitronyl Nitroxides

Ekaterina Kudryavtseva [1], Andrey Serykh [1,2], Bogdan Ugrak [1], Tatyana Dutova [1], Darina Nasyrova [1], Alexander Korlyukov [3], Mikhail Zykin [4], Nikolay Efimov [4], Artem Bogomyakov [5] and Evgeny Tretyakov [1,*]

[1] N. D. Zelinsky Institute of Organic Chemistry, Leninsky Ave. 47, Moscow 119991, Russia
[2] D. Mendeleev University of Chemical Technology of Russia, Miusskaya Pl. 9, Moscow 125047, Russia
[3] A. N. Nesmeyanov Institute of Organoelement Compounds, 28 Vavilov Str., Moscow 119991, Russia
[4] N. S. Kurnakov Institute of General and Inorganic Chemistry, Leninsky Ave. 31, Moscow 119991, Russia
[5] International Tomography Center, Siberian Branch of Russian Academy of Sciences, Institutskaya Str. 3a, Novosibirsk 630090, Russia
* Correspondence: tretyakov@ioc.ac.ru

Abstract: New complexes of manganese(II) hexafluoroacetylacetonate [Mn(hfac)$_2$] with 2-(1-*R*-3-pyrazol-4-yl)-4,4,5,5-tetramethyl-2-imidazoline-3-oxide-1-oxyl (*R* = CHF_2, CH_2CH_2F, CH_2CHF_2 or CH_2CF_3) were synthesised and characterised structurally and magnetically. All complexes were prepared under similar conditions. Nonetheless, their crystal structures were considerably different. Depending on the structure of fluorinated alkyl substituent *R*, the complexation reaction led to complexes of three types: chain-polymeric complexes with the head-to-head or head-to-tail motif and complexes of molecular structure. All complexes show strong antiferromagnetic behaviour in a high-temperature region (150–300 K) and weak ferro- or antiferromagnetic exchange interactions at low temperatures. The stronger antiferromagnetic exchange, –101.7 ± 1.5 or –136 ± 10 cm^{-1}, –82.3 ± 1.3 cm^{-1} and –87.4 ± 1.3 cm^{-1}, was attributed to the magnetic interaction in three- or two-spin clusters: {>N ÷ O–Mn^{2+}–O ÷ N<} or {>N ÷ O–Mn^{2+}}, respectively. The weaker antiferromagnetic interaction, –0.005, between three-spin clusters or ferromagnetic interactions, 0.18–0.81 cm^{-1}, between two-spin clusters are realised through the pyrazole ring or intermolecular contacts.

Keywords: nitronyl nitroxides; metal-nitroxide complexes; crystal structures; magnetic properties

1. Introduction

Nitroxide radicals have been proved to be promising ligands for the construction of molecular magnetic materials [1–4]. The ease of modification of nitronyl nitroxide radicals gives versatility to the design of various interesting systems of the metal–nitroxide type. Such systems have a large variety of topological structures and manifest intriguing bulk and molecular magnetic properties [5–12]. The direct linking of nitronyl nitroxides to metal ions results in the strongest possible magnetic coupling, which reduces quantum tunnelling of the magnetisation and gives long relaxation time [13,14]. So far, a number of molecular magnets based on metal–nitroxide complexes have been created, for example, cobalt-radical coordination magnets with high coercivity blocking temperature [15–17]. In addition, discrete complexes with defined geometric structure of paramagnetic metal ions and nitronyl nitroxide radical ligands are good candidates for basic research on magneto-structural correlations [18–20].

In a preceding paper, we investigated an influence of step-by-step fluorination of different paramagnetic systems on their structure and magnetism [21–28]. The motivation was that the introduction of fluorine atom(s) into molecules alters physical and chemical properties of the compounds because of fluorine's electronegativity, its low polarisability and high bond strength [29].

Preprints (www.preprints.org) | NOT PEER-REVIEWED | Posted: 26 September 2023 doi:10.20944/preprints202309.1700.v1

In addition, there are many examples of the influence of substitution with fluorine on inter-molecular interactions and the use of 'organic fluorine' in crystal engineering or in systematic design of functional materials [30–34]. Many research groups have performed comprehensive analyses of crystal structures of fluorine-containing compounds and published excellent reviews on the specific role of fluorine in crystal packing [35,36]. In some reviews, fluorine has been poetically described as the odd man out [37], the little atom that could [29], the atom with many faces [38], and the chameleon of noncovalent interactions [39]. Although there is ample research on inter-molecular interactions of the C–F group in various types of compounds, this kind of interactions has not been studied in a systematic series of complexes of paramagnetic metal ions with radicals. Intuitively, it is expected that the introduction of fluorine into metal–radical systems can have a significant influence on their packing in the crystals thereby changing inter-molecular exchange interaction channels and eventually magnetic characteristics of molecular magnetic materials.

Herein, we used a series pyrazolyl-substituted nitronyl nitroxides bearing different fluorinated alkyl groups in the pyrazole nucleus, namely 2-(1-*R*-3-pyrazol-4-yl)-4,4,5,5-tetramethyl-2-imidazoline-3-oxide-1-oxyl, where *R* = CHF_2, CH_2CH_2F, CH_2CHF_2 or CH_2CF_3. The complexation reaction of $[Mn(hfac)_2]$ with these radicals under identical conditions led to the formation of complexes of dimer structure, head-to-head chain-polymeric structure or head-to-tail chain-polymeric structure depending on the structure of the fluorinated alkyl substituent. Magnetic analyses showed that there is a strong antiferromagnetic interaction between the Mn(II) ion and the directly coordinated N–O group in the high-temperature region and weak ferro- or antiferromagnetic exchange interactions below 100 K.

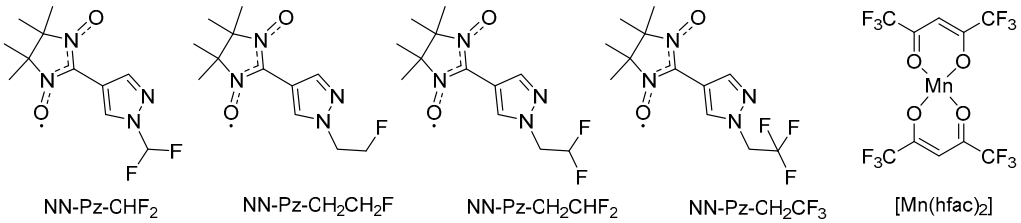

2. Materials and Methods

2.1. General procedures and materials

2-(1-*R*-3-Pyrazol-4-yl)-4,4,5,5-tetramethyl-2-imidazoline-3-oxide-1-oxyls (L^R), where *R* = CHF_2, CH_2CH_2F, CH_2CHF_2 or CH_2CF_3, were synthesised according to methods from the literature [25]. All other chemicals were of reagent grade and used without purification. Toluene was distilled under an argon stream and kept in an argon atmosphere. Other solvents were of reagent quality and used without additional purification. The reactions were monitored by thin-layer chromatography on silica gel 60 F_{254} aluminium sheets from Merck. The chromatography was carried out using silica gel (0.050–0.160 mm) for column chromatography. The yields are given for pure substances obtained after recrystallisation. IR spectra were obtained from KBr pellets by means of a Bruker VECTOR 22 infrared spectrometer. Elemental analyses for C, H and N were carried out using Perkin-Elmer elemental analyzer model 240.

2.2. Synthesis of $[Mn(hfac)_2(NN\text{-}Pz\text{-}CHF_2)]_n$

A solution of 42 mg (0.08 mmol) of $Mn(hfac)_2{\cdot}2H_2O$ in 5 mL of dry toluene was heated under reflux for 40 min. After that, the solution was cooled to the room temperature, and a solution of NN-Pz-CHF_2 (22 mg, 0.08 mmol) in 1 mL of toluene was added. The resulting mixture was allowed to stand at –15 °C for a week to obtain blue blocks of crystals (30.9 mg, 57.5%). Anal. calcd. for $C_{21}H_{17}F_{14}MnN_4O_6$: C, 33.98; H, 2.31; N, 7.55. Found: C, 33.99; H, 2.20; N, 7.57%. IR (KBr, cm^{-1}): 3149(m), 2997(m), 2947(w), 1645(s), 1611(m), 1562(m), 1536(m), 1501(s), 1488(s), 1466(m), 1407(m), 1395(m), 1381(m), 1348(s), 1328(s), 1260(s), 1223(s), 1142(s), 1099(s), 1020(m), 1002(w), 965(w), 946(w), 892(m),

 doi:10.20944/preprints202309.1700.v1

869(m), 838(s), 807(s), 766(w), 742(m), 697(w), 666(s), 609(w), 585(m), 542(m), 528(w), 483(w),470(w), 419(w).

2.3. Synthesis of [Mn(hfac)$_2$(NN-Pz-CH$_2$CH$_2$F)]$_n$

A solution of 42 mg (0.08 mmol) of Mn(hfac)$_2$·2H$_2$O in 5 mL of dry toluene was heated under reflux for 40 min. Next, the solution was cooled to room temperature, and a solution of NN-Pz-CH$_2$CH$_2$F (22 mg, 0.08 mmol) in 1 mL of toluene was introduced. The resulting mixture was kept at –15 °C for several days to obtain blue blocks of crystals (32.2 mg, 52.4% based on Mn ion). Anal. calcd. for $C_{22}H_{20}F_{13}MnN_4O_6$: C, 35.79; H, 2.73; N, 7.59. Found: C, 35.52; H, 2.71; N, 7.81%. IR (KBr, cm^{-1}): 3153(m), 2996(w), 1649(s), 1610(w), 1556(w), 1530(m), 1500(m), 1350(m), 1301(w), 1257(s), 1206(s), 1146(s), 1097(w), 1039(w), 1019(w), 884(w), 863(w), 798(m), 758(w), 741(w), 665(m), 584(m), 544(w), 527(w), 507(w), 464(w), 435(w).

2.4. Synthesis of [Mn(hfac)$_2$(NN-Pz-CH$_2$CHF$_2$)]$_n$·nC$_7$H$_8$ and [Mn(hfac)$_2$(NN-Pz-CH$_2$CHF$_2$)]$_n$

A solution of 42 mg (0.08 mmol) of Mn(hfac)$_2$·2H$_2$O in 5 mL of dry toluene was heated under reflux for 40 min. Then, the solution was cooled to room temperature, and a solution of NN-Pz-CH$_2$CHF$_2$ 23 mg (0.08 mmol) in 1 mL of toluene was added. The resultant mixture was incubated at –15 °C for ~20 h to obtain blue blocks of crystals of solvate complex [Mn(hfac)$_2$(NN-Pz-CH$_2$CHF$_2$)]$_n$·nC$_7$H$_8$. The crystals were filtered off and dried on air. Yield 40.9 mg (60.2%). The complex [Mn(hfac)$_2$(NN-Pz-CH$_2$CHF$_2$)]$_n$·nC$_7$H$_8$ was stored for a month in vial at ambient condition that led to its desolvation. Anal. calcd. for $C_{22}H_{19}F_{14}MnN_4O_6$: C, 34.94; H, 2.53; N, 7.41. Found: C, 34.78; H, 2.60; N, 8.18%. IR (KBr, cm^{-1}): 3152(m), 2996(w), 2948(w), 1646(s), 1611(m), 1559(m), 1532(s), 1501(s), 1401(w), 1353(s), 1373 sh, 1320(w), 1303(w), 1259(s), 1214(s), 1192 sh, 1144(s), 1090(s), 1069(m), 1019(w), 1007(w), 946(w), 886(w), 867(w), 798(m), 742(w), 666(s), 642(w), 605(w), 585(m), 558(w), 544(w), 527(w), 484(w), 469(w), 436(w).

2.5. Synthesis of [Mn(hfac)$_2$(NN-Pz-CH$_2$CF$_3$)]$_2$·2C$_7$H$_8$

A solution of 34 mg (0.07 mmol) of Mn(hfac)$_2$·2H$_2$O in 5 mL of dry toluene was heated under reflux for 40 min. After that, the solution was cooled to room temperature, and a solution of NN-Pz-CH$_2$CF$_3$ 22 mg (0.07 mmol) in 3 mL of toluene was added. This mixture was allowed to stand at –15 °C for ~24 h to obtain blue blocks of crystals (44.5 mg, 76.3%). Anal. calcd. for $C_{44}H_{36}F_{30}Mn_2N_8O_{12}$·2($C_7H_8$): C, 40.20; H, 3.02; N, 6.47. Found: C, 40.12; H, 3.01; N, 6.31%. IR (KBr, cm^{-1}): 3153(m), 3024(w), 2996(w), 2948(w), 1647(s), 1610(m), 1558(m), 1532(m), 1501(s), 1481 sh, 1438 sh, 1400(w), 1356(m), 1315(m), 1257(s), 1197(s), 1146(s), 1096 sh, 1020(m), 933(m), 889(w), 868(w), 841(w), 800(m), 766(w), 742(w), 664(m), 584(m), 542(w), 469(w), 433(w).

2.6. X-ray Crystallography Details

X-ray diffraction (XRD) data on monocrystals of [Mn(hfac)$_2$(NN-Pz-CHF$_2$)]$_n$, [Mn(hfac)$_2$(NN-Pz-CH$_2$CH$_2$F)]$_n$, [Mn(hfac)$_2$(NN-Pz-CH$_2$CHF$_2$)]$_n$·nC$_7$H$_8$ and [Mn(hfac)$_2$(NN-Pz-CH$_2$CF$_3$)]$_2$·2C$_7$H$_8$ were collected at 100 K on a four-circle Rigaku Synergy S diffractometer equipped with a HyPix6000HE area-detector (kappa geometry, shutterless ω-scan technique) using mono-chromatised Cu K$_\alpha$-radiation. The intensity data were integrated and corrected for absorption and decay in the CrysAlisPro software [40]. The structures were solved by direct methods using SHELXT [41] and refined on F^2 with the help of SHELXL-2018 [42] in OLEX2 [43]. All non-hydrogen atoms were refined with individual anisotropic displacement parameters. All hydrogen atoms were placed in ideal calculated positions and refined as riding atoms with relative isotropic displacement parameters. A rotating group model was applied to methyl groups.

XRD data on monocrystals of [Mn(hfac)$_2$(NN-Pz-CH$_2$CHF$_2$)]$_n$ and [Mn(hfac)$_2$(NN-Pz-CH$_2$CHF$_2$)]$_n$ n[Mn(hfac)$_2$(NN-Pz-CH$_2$CHF$_2$)H$_2$O]) were collected at 100 K on a Bruker D8 QUEST diffractometer. Single-crystal X-ray analyses were carried out in the APEX3 software [44]. The

collected data were then integrated in SAINT. SADABS was used for scaling, empirical absorption corrections and for generating data files for structure solution and refinement.

CCDC 2272057 (for $[Mn(hfac)_2(NN\text{-}Pz\text{-}CHF_2)]_n$), 2272056 (for $[Mn(hfac)_2(NN\text{-}Pz\text{-}CH_2CH_2F)]_n$), 2239233 (for $[Mn(hfac)_2(NN\text{-}Pz\text{-}CH_2CHF_2)]_n$), 2239234 for $[Mn(hfac)_2(NN\text{-}Pz\text{-}CH_2CHF_2)]_n$ n$[Mn(hfac)_2(NN\text{-}Pz\text{-}CH_2CHF_2)H_2O]$), 2272055 $[Mn(hfac)_2(NN\text{-}Pz\text{-}CH_2CHF_2)]_n{\cdot}nC_7H_8$ and 2272058 (for $[Mn(hfac)_2(NN\text{-}Pz\text{-}CH_2CF_3)]_2{\cdot}2C_7H_8$) contain the supplementary crystallographic data for the manganese–nitroxide complexes.

2.7. Magnetic measurements

The variable-temperature magnetic-susceptibility measurements were carried out in the temperature range 2–300 K with a Quantum Design PPMS-9 or Quantum Design MPMSXL SQUID magnetometer. None of the complexes showed any field dependence of molar magnetic susceptibility at low temperatures. The molar magnetic susceptibility was corrected for the sample holder and diamagnetic contributions of all constituent atoms by means of Pascal's constants [45].

3. Results and discussion

3.1. Synthesis and crystal structures of manganese–nitroxide complexes

Complexes $[Mn(hfac)_2(NN\text{-}Pz\text{-}R)]_n$ were prepared by interaction of manganese(II) hexafluoroacetylacetonate ($[Mn(hfac)_2]$) with nitronyl nitroxides (NNs), namely 2-(1-*R*-3-pyrazol-4-yl)-4,4,5,5-tetramethyl-2-imidazoline-3-oxide-1-oxyls (*R* = CHF_2, CH_2CH_2F, CH_2CHF_2 or CH_2CF_3), in dry toluene at –15 °C. The single-crystal X-ray analysis revealed that compound $[Mn(hfac)_2(NN\text{-}Pz\text{-}CHF_2)]_n$ crystallises in orthorhombic space group *I*2/a. The structure of $[Mn(hfac)_2(NN\text{-}Pz\text{-}CHF_2)]_n$ consists of 1D coordination chains shown in Figure 1a. One can see that the paramagnetic NN-Pz-CHF_2 is a bridging bidentate ligand coordinated via the oxygen atom of one of the N–O groups and the nitrogen atom of the pyrazole ring. The coordination chains have a 'head-to-head' motif, and the nitroxide oxygen atoms and the nitrogen atom are coordinated to Mn in a *trans*-configuration. Each manganese ion is sixfold coordinated and has almost isometric octahedral geometry. For the MnO_6 unit, the $Mn–O_{NO}$ bond lengths are 2.143 Å, whereas the average $Mn–O_{hfac}$ bond length is 2.139 Å. These values are close to those observed for other complexes of $[Mn(hfac)_2]$ with nitronyl nitroxides [46,47]. For the MnO_4N_2 unit, the Mn–N bond lengths are 2.297 Å, whereas the $Mn–O_{hfac}$ bond lengths are 2.132 and 2.138 Å. In the coordinated nitroxide group, the bond length [1.303(2) Å] is slightly elongated as compared with the non-coordinated one [1.273(2) Å]. The shortest inter-chain distances between O atoms of the nitroxide groups exceed 5 Å (the sum of van der Waals radii of O atoms is 3.04 Å); this arrangement allows one to expect only very weak exchange interactions between the chains.

Preprints (www.preprints.org) | NOT PEER-REVIEWED | Posted: 26 September 2023 doi:10.20944/preprints202309.1700.v1

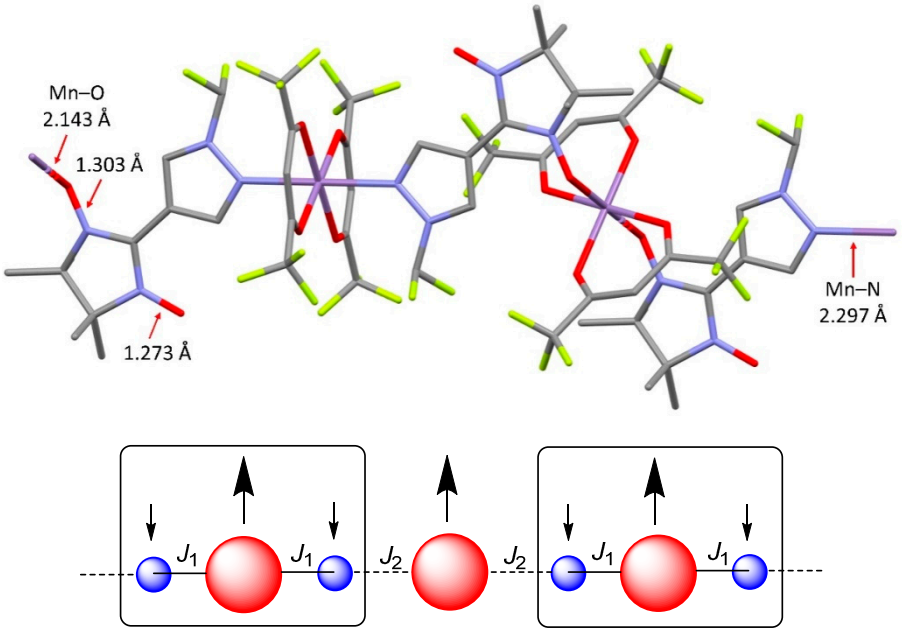

Figure 1. (**a**) A fragment of chain structure in $[Mn(hfac)_2(NN\text{-}Pz\text{-}CHF_2)]_n$ (colour code: Mn: violet, N: blue, O: red, F: yellow, C: gray; H atoms are not shown for the sake of clarity). (**b**) Magnetic exchange pathways within and between the repeating units (the red and blue balls denote the $S_{Mn} = 5/2$ and $S_R = 1/2$ spins, respectively; the arrows indicate the spin alignment in the ground state).

Figure 1b shows a schematic diagram of possible magnetic interactions within the manganese–nitroxide chains; the direct coordination bonding of two O atoms to Mn(II) should give the largest exchange interaction, which is denoted as J_1, whereas magnetic couplings between Mn(II) ions and the nitroxide group via the pyrazole ring (denoted as J_2) should be weaker than J_1. The sign and magnitude of these interactions are discussed in the Magnetic Properties section.

Complex $[Mn(hfac)_2(NN\text{-}Pz\text{-}CH_2CH_2F)]_n$ was found to crystallise in monoclinic space group $P2_1/c$. The structure of $[Mn(hfac)_2(NN\text{-}Pz\text{-}CH_2CH_2F)]_n$ also consists of 1D coordination chains (Figure 2) formed by bridging bidentate ligand coordination via the nitroxide O atom and the N atom of the pyrazole ring. As opposed to $[Mn(hfac)_2(NN\text{-}Pz\text{-}CHF_2)]_n$, the coordination chains have a head-to-tail motif, and the nitroxide O atom and N atom are coordinated to Mn in a *cis*-configuration. The coordination polyhedron of manganese is nearly isometric. The Mn–O_{NO} bond length is 2.145(2) Å, the Mn–N bond length is 2.236(2) Å, whereas the Mn–O_{hfac} bond lengths are 2.130(2), 2.144(2), 2.172(2) and 2.176(2) Å. In the coordinated nitroxide group, the bond length [1.305(3) Å] is slightly elongated as compared with the non-coordinated one [1.278(3) Å]. The shortest inter-chain distance between the oxygen atoms of nitroxide groups is 4.266 Å, which is also considerably greater than the sum of van der Waals radii of O atoms (3.04 Å).

Preprints (www.preprints.org) | NOT PEER-REVIEWED | Posted: 26 September 2023 doi:10.20944/preprints202309.1700.v1

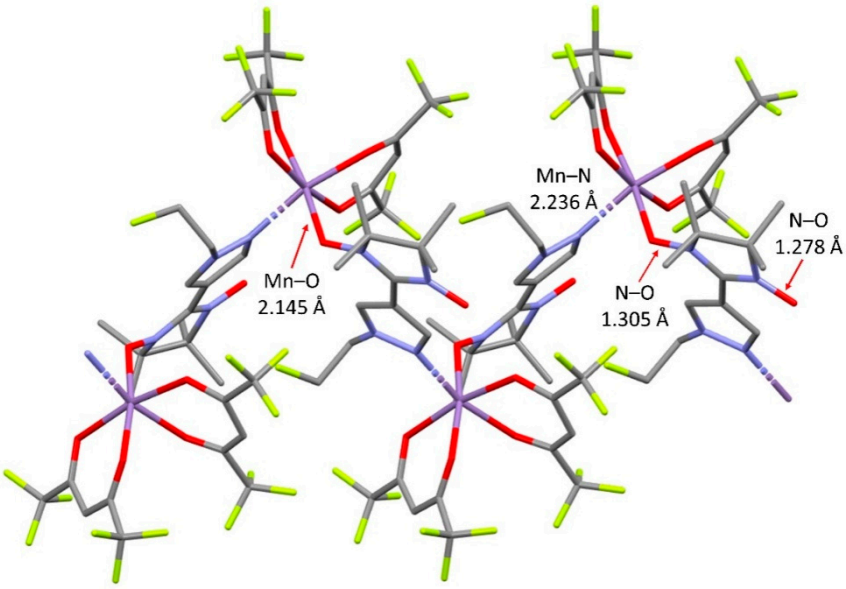

Figure 2. A fragment of chain structure in $[Mn(hfac)_2(NN\text{-}Pz\text{-}CH_2CH_2F)]_n$ (colour code: Mn: violet, N: blue, O: red, F: yellow, C: gray; H atoms are not shown for the sake of clarity).

The interaction of $[Mn(hfac)_2]$ with NN-Pz-CH_2CHF_2 in dry toluene at –15 °C gave rise to complex $[Mn(hfac)_2(NN\text{-}Pz\text{-}CH_2CHF_2)]_n \cdot nC_7H_8$ in the form of a solvate with toluene. Complex $[Mn(hfac)_2(NN\text{-}Pz\text{-}CH_2CHF_2)]_n \cdot nC_7H_8$ was found to crystallise in the same monoclinic space group, $P2_1/n$. The structure of $[Mn(hfac)_2(NN\text{-}Pz\text{-}CH_2CHF_2)]_n$ also consists of 1D coordination chains (Figure 3) with the head-to-tail motif and *cis*-configuration of the Mn surroundings. The coordination of the manganese polyhedron is nearly isometric: the Mn–O_{NO} bond length is 2.138(3) Å, the Mn–N bond length is 2.245(3) Å whereas the Mn–O_{hfac} bond lengths lie in the range 2.126(2)–2.169(2) Å. In the coordinated nitroxide group, the bond length [1.309(4) Å] is slightly elongated as compared with the non-coordinated one [1.274(4) Å]. The shortest inter-chain distances between the oxygen atoms of nitroxide groups exceed 5.0 Å. After storage under ambient conditions, the complex $[Mn(hfac)_2(NN\text{-}Pz\text{-}CH_2CHF_2)]_n \cdot nC_7H_8$ loses the solvate molecules while retaining the quality of the crystals. According to XRD data, crystal structure of desolated complex $[Mn(hfac)_2(NN\text{-}Pz\text{-}CH_2CHF_2)]_n$ belongs to space group $P2_1/c$. In $[Mn(hfac)_2(NN\text{-}Pz\text{-}CH_2CHF_2)]_n$, geometric parameters are almost the same as in its solvate with toluene, for example, the Mn–O_{NO} bond length is 2.147(2) Å, and the Mn–N bond length is 2.247(2) Å, whereas the Mn–O_{hfac} bond lengths lie in the range 2.126(2)–2.178(2) Å. N–O bond lengths are 1.310(3) and 1.277(3) Å for coordinated and non-coordinated nitroxide groups, respectively (Figure S1).

In accordance with the structure of complexes $[Mn(hfac)_2(NN\text{-}Pz\text{-}CH_2CH_2F)]_n$ and $[Mn(hfac)_2(NN\text{-}Pz\text{-}CH_2CHF_2)]_n$, there are two kinds of magnetic interactions in the chains: Mn(II)–nitroxide direct magnetic interactions, J_1, and Mn(II)–nitroxide interactions through the pyrazole ring: J_2 (Figure 3b). It is known that nitroxide radicals directly bound to Mn(II) centres through the N–O group always exhibit much stronger magnetic coupling than that through a donor atom of the nitronyl nitroxide substituent [48–50]. Therefore, from a magnetic point of view, the coordination chain can be described as strongly coupled two-spin clusters with relatively weak exchange between them: J_2. The quantification of these magnetic interactions is discussed in the Magnetic Properties section.

Preprints (www.preprints.org) | NOT PEER-REVIEWED | Posted: 26 September 2023 doi:10.20944/preprints202309.1700.v1

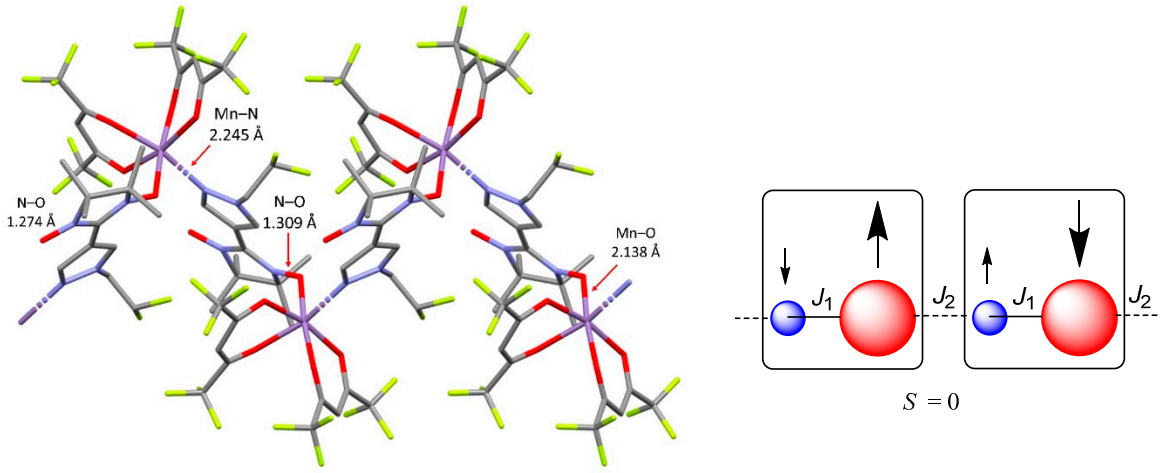

Figure 3. (**a**) A fragment of chain structure in $[Mn(hfac)_2(NN\text{-}Pz\text{-}CH_2CHF_2)]_n \cdot nC_7H_8$ (colour code: Mn: violet, N: blue, O: red, F: yellow, C: gray; the solvate molecules and H atoms are not shown). (**b**) Magnetic exchange pathways within and between the two spin clusters (the red and blue balls denote the S_{Mn} = 5/2 and S_R = 1/2 spins, respectively; the arrows indicate the spin alignment in the ground state).

The reaction of $Mn(hfac)_2$ with $NN\text{-}Pz\text{-}CH_2CF_3$ led to the formation solvate complex $[Mn(hfac)_2(NN\text{-}Pz\text{-}CH_2CF_3)]_2 \cdot 2C_7H_8$ having structure of a cyclic dimer (Figure 4). Crystal structure of the complex belongs to the triclinic *P*-1 space group. The structure of the complex results from the bridging bidentate ligand coordination via the nitroxide O atom and the N atom of the pyrazole ring. The Mn–O_{NO} bond length is 2.110(2) Å, and the Mn–N bond length is 2.278(2) Å, which are comparable to those observed in previously reported cyclic metal–nitroxide dimers [51–53]. In the coordinated nitroxide group, the bond length is also slightly elongated [1.303(2) Å] as compared with the non-coordinated one [1.272(3) Å]. The Mn···Mn distance in the intra-dimer is 6.248 Å, which is shorter than the shortest inter-dimer Mn···Mn distance of 8.984 Å. The shortest distances between the uncoordinated NO groups is 4.886 Å. The packing diagram for $[Mn(hfac)_2(NN\text{-}Pz\text{-}CH_2CF_3)]_2 \cdot 2C_7H_8$ is shown in Figure S2. The cyclic dimers are arranged parallel to each other along the a-axis thereby forming stacks, between which the shortest contacts that are established by oxygen atoms (O1) of the uncoordinated nitroxide groups and hydrogen atoms (H6C) of methyl groups are 2.532 Å. It is also noteworthy that unlike complex $[Mn(hfac)_2(NN\text{-}Pz\text{-}CH_2CHF_2)]_n \cdot nC_7H_8$, solvate complex $[Mn(hfac)_2(NN\text{-}Pz\text{-}CH_2CF_3)]_2 \cdot 2C_7H_8$ is stable under ambient conditions and does not lose the solvent molecules.

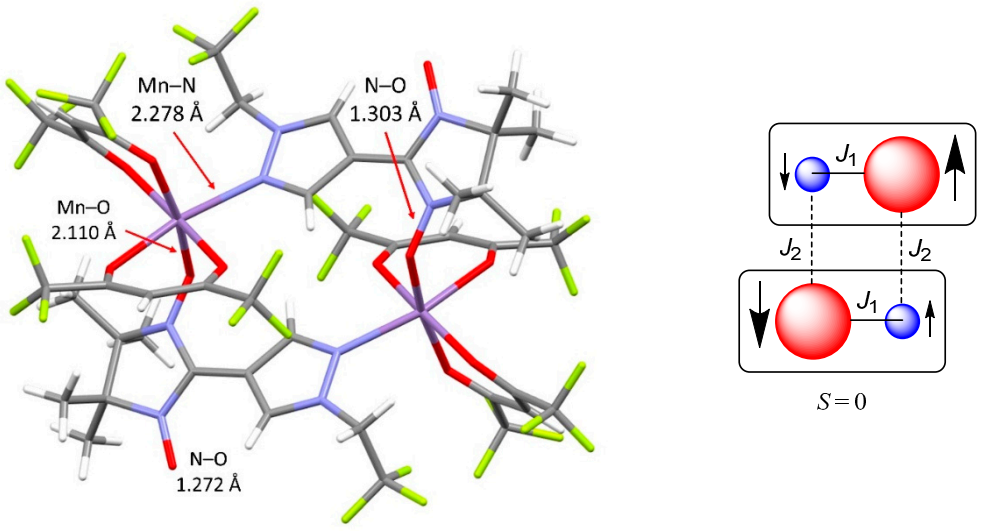

Preprints (www.preprints.org) | NOT PEER-REVIEWED | Posted: 26 September 2023 doi:10.20944/preprints202309.1700.v1

(**a**) (**b**)

Figure 4. (**a**) The cyclic dimer in the structure of $[Mn(hfac)_2(NN\text{-}Pz\text{-}CH_2CF_3)]_2 \cdot 2C_7H_8$ (colour code: Mn: violet, N: blue, O: red, F: yellow, C: gray; the solvate molecules and H atoms are not shown). (**b**) Magnetic exchange pathways within the dimer (the red and blue balls represent the $S_{Mn} = 5/2$ and $S_R = 1/2$ spins, respectively; the arrows indicate the spin alignment in the ground state).

In $[Mn(hfac)_2(NN\text{-}Pz\text{-}CH_2CF_3)]_2$, there are mainly two kinds of magnetic interactions for the present four-spin magnetic system, i.e. the magnetic interaction between the Mn(II) ion and the directly coordinated nitroxide group (J_1) and the magnetic coupling between the Mn(II) ion and nitroxide group through the pyrazole rings (J_2) (Figure 4b). The second kind of magnetic coupling will be shown below to be weak and ferromagnetic (see the Magnetic Properties section).

The experimental powder XRD patterns of all complexes matched well the simulated XRD patterns based on the structures refined by single-crystal XRD analysis. In addition, elemental analyses yielded satisfactory results for all manganese–nitroxide complexes. The preparation of the complexes and their characterisation were repeated at least three times; the results (yields, crystal structures) were reproducible.

Notably, the reaction of $[Mn(hfac)_2]$ with NN-Pz-R^F under the same conditions produced complexes of different types: a chain-polymeric complex with a head-to-head motif or head-to-tail motif as well as molecular complex. The reason is a fine influence of fluorinated alkyl substituents R in NN-Pz on a set of equilibrium constants predetermining concentrations of different species and their solubility (Scheme 1). In NN-Pz-CH_2CF_3, the fluoroalkyl substituent somewhat reduces electron density on the donor nitrogen atom, and this effect obviously should favour the formation of a soluble Pz-NN–{Mn} complex with a coordinated NO group. If we assume that the acceptor ability of the manganese atom in Pz-NN–{Mn} is not sufficient to bind one more ligand, then the formation of a cyclic dimer with pairwise coordination bonds becomes preferable and therefore leads to precipitation of $[Mn(hfac)_2(NN\text{-}Pz\text{-}CH_2CF_3)]_2$. Incidentally, the reasons may be the same for the frequent formation of such dimers during the interaction of $[Mn(hfac)_2]$ with hetaryl-substituted nitronyl nitroxides [54–59].

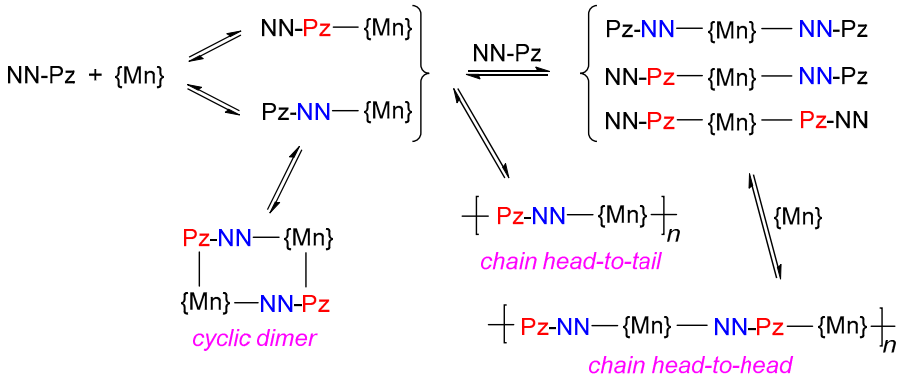

Scheme 1. Plausible pathways to different Mn–nitroxide complexes.

On the contrary, only one case is known when the reaction of $[Mn(hfac)_2]$ with a hetaryl-substituted nitronyl nitroxide produces a chain-polymeric complex, moreover, having a head-to-head motif [60]. In our case, the $[Mn(hfac)_2(NN\text{-}Pz\text{-}CHF_2)]_n$ complex has similar structure, and its formation can be explained by the influence of the CHF_2 substituent, which reduces electron density on the donor nitrogen atom to such an extent that the formation of the corresponding dimer becomes thermodynamically unfavourable. Therefore, the process goes further along the path of coordination of another radical by the manganese ion through the NO group with the formation of a three-spin molecule: Pz-NN–{Mn}–NN-Pz. The interaction of the latter with the $[Mn(hfac)_2]$ acceptor matrix eventually gives a poorly soluble chain-polymeric complex with a head-to-head motif (Scheme 1). Incidentally, one can notice an interesting detail: only in this case does the complex precipitate into a solid phase very slowly (for approximately a week), whereas solid phases of the other complexes

Preprints (www.preprints.org) | NOT PEER-REVIEWED | Posted: 26 September 2023 doi:10.20944/preprints202309.1700.v1

described here form much faster, within several hours. This finding indirectly indicates that the concentration of the Pz-NN–{Mn}–NN-Pz form that is necessary for the assembly of the solid phase of the $[Mn(hfac)_2(NN\text{-}Pz\text{-}CHF_2)]_n$ complex is too low in the solution.

The structure of the two remaining complexes, $[Mn(hfac)_2(NN\text{-}Pz\text{-}CH_2CH_2F)]_n$ and $[Mn(hfac)_2(NN\text{-}Pz\text{-}CH_2CHF_2)]_n$, is unprecedented. These are the first examples of manganese–nitroxide chain-polymeric complexes with a head-to-tail motif in which hetaryl-substituted nitronyl nitroxides serve as bidentate-bridging ligands. Their formation can be explained as follows: a decrease in electron acceptor properties of substituent R possibly enhances the donor ability of the nitrogen atom of the paramagnetic ligand to such an extent that the NN-Pz–{Mn} complex becomes preferable in solution, thereby causing crystallisation of the chain head-to-tail complexes (Scheme 1).

The effect of R^F substituents on the course of the complexation reactions can also be observed visually. As mentioned above, the $[Mn(hfac)_2(NN\text{-}Pz\text{-}CHF_2)]_n$ complex precipitates very slowly, and after 24 h, one can see the emergence of a small amount of the product (Figure 5). In case of $[Mn(hfac)_2(NN\text{-}Pz\text{-}CH_2CH_2F)]_n$, after 24 h under the same conditions, a gel-like product initially arises, retaining the entire mother liquor. This product, upon further incubation of the reaction mixture for several days, transitions to a crystalline $[Mn(hfac)_2(NN\text{-}Pz\text{-}CH_2CH_2F)]_n$ complex. The two latter complexes, $[Mn(hfac)_2(NN\text{-}Pz\text{-}CH_2CH_2F)]_n$ and $[Mn(hfac)_2(NN\text{-}Pz\text{-}CH_2CHF_2)]_n$, form faster and after 24 h almost completely precipitate with the emergence of crystalline phases.

(**a**) (**b**)

Figure 5. Images of inverted reaction vessels with reaction mixtures $[Mn(hfac)_2]$ + NN-Pz-CHF_2 (**a**) and $[Mn(hfac)_2]$ + NN-Pz-CH_2CH_2F (**b**) after incubation at –15 °C for 24 h.

Thus, the fluorinated substituents in NN-Pz have a substantial effect on the structure of heterospin manganese–nitroxide complexes. It is noteworthy that their solid phases have different sets of exchange channels, and therefore a difference in magnetic behaviour is expected.

3.2. Magnetic properties

The temperature dependence of effective magnetic moment μ_{eff} for $[Mn(hfac)_2(NN\text{-}Pz\text{-}CHF_2)]_n$ is shown in Figure 6. The μ_{eff} value at 300 K is 5.17 μ_B and slightly decreases to reach a plateau of 4.99 μ_B in the temperature range 150–10 K. The observed μ_{eff} values in the temperature range 10–300 K are considerably less than the theoretical spin-only value of 6.16 μ_B for the non-interacting spin system of Mn^{2+} and nitroxide based on the $\{Mn(hfac)_2(NN\text{-}Pz\text{-}CHF_2)\}$ moiety. It is reasonable to explain the observed magnetic behaviour of $[Mn(hfac)_2(NN\text{-}Pz\text{-}CHF_2)]_n$ by the strong antiferromagnetic interactions in $\{>N \div O–Mn^{2+}–O \div N<\}$ three-spin exchange clusters, in which the spins of the coordinated N÷O groups partially compensate the spin of the Mn^{2+} ion (S_{Mn} = 5/2). In the range from 150 to 10 K, the μ_{eff} values are close to theoretical value $\mu_{teor} = (0.5{\cdot}15 + 0.5{\cdot}35)^{1/2} = 5$ μ_B, taking into account that the magnetic susceptibility contains contributions only from residual moments of the three-spin exchange clusters having a quartet ground state (S = 3/2) and from the moments of the Mn^{2+} ions located in MnO_4N_2 coordination units (S_{Mn} = 5/2). The decline of μ_{eff} below 10 K down to 4.69 μ_B at 2 K is explained by the weak inter-chain antiferromagnetic interactions (Figure 1b). Analysis of the experimental $\mu_{eff}(T)$ dependence, using a trimer model for the $\{>N \div O–Mn^{2+}–O \div N<\}$ exchange

Preprints (www.preprints.org) | NOT PEER-REVIEWED | Posted: 26 September 2023 doi:10.20944/preprints202309.1700.v1

cluster (spin-Hamiltonian $H = -2J(S_{R1}S_{Mn} + S_{Mn}S_{R2})$) while taking into account magnetic susceptibility of the Mn^{2+} ions located in MnO_4N_2 coordination units according to Curie law, allows to estimate exchange interaction energy. The best-fit values of g-factors and exchange interaction parameter J are 2.01 ± 0.01 and –101.7 ± 1.5 cm^{-1}, respectively. The weaker exchange interactions, J_n, are approximated as mean-field parameter θ thus giving –0.005 ± 0.001 cm^{-1}.

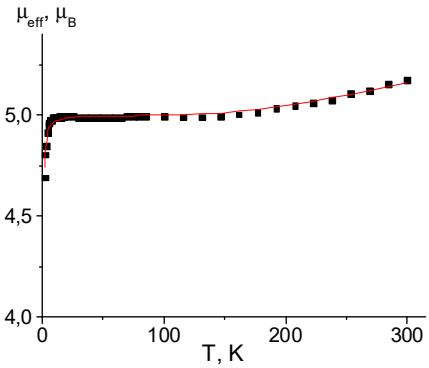

Figure 6. The temperature dependence of μ_{eff} for complex $[Mn(hfac)_2(NN\text{-}Pz\text{-}CHF_2)]_n$. The solid curve corresponds to the best theoretical fit.

For complexes $[Mn(hfac)_2(NN\text{-}Pz\text{-}CH_2CH_2F)]_n$ and $[Mn(hfac)_2(NN\text{-}Pz\text{-}CH_2CHF_2)]_n$ with a head-to-tail motif of chains, the $\mu_{eff}(T)$ dependences are similar (Figure 7). The μ_{eff} values are 5.34 and 5.37 μ_B and slightly decrease with diminishing temperature. The μ_{eff} values in the temperature range 300–50 K are close to the theoretical spin-only value of 4.90 μ_B for one paramagnetic centre with $S = 2$, indicating realisation of strong antiferromagnetic exchange interactions in {Mn^{2+}–O˙˙N<} exchange clusters. Below 50 K, μ_{eff} values drop rapidly, which is caused by the weak inter-cluster interactions within the chains. Analysis of the experimental $\mu_{eff}(T)$ dependences using two-spin model (spin-Hamiltonian $H = -2JS_{Mn}S_R$) as reported in ref. [61] enabled us to estimate exchange interaction energy in {Mn^{2+}–O ˙˙ N<} exchange clusters. The best-fit values of g-factors and exchange interaction parameter J_1 (see Figure 3b) are 2.029 ± 0.003 and –136 ± 10 cm^{-1} for $[Mn(hfac)_2(NN\text{-}Pz\text{-}CH_2CH_2F)]_n$, and 2.041 ± 0.002 and –82.3 ± 1.3 cm^{-1}, respectively, for $[Mn(hfac)_2(NN\text{-}Pz\text{-}CH_2CHF_2)]_n$. The weak exchange interactions between paramagnetic centers are approximated as mean-field parameter θ thus giving 0.78 ± 0.01 cm^{-1} and 0.18 ± 0.01 cm^{-1}, respectively. The small positive value of θ may be attributed with FM exchange between the Mn(II) ion and the nitronyl nitroxide moiety through the pyrazole ring.

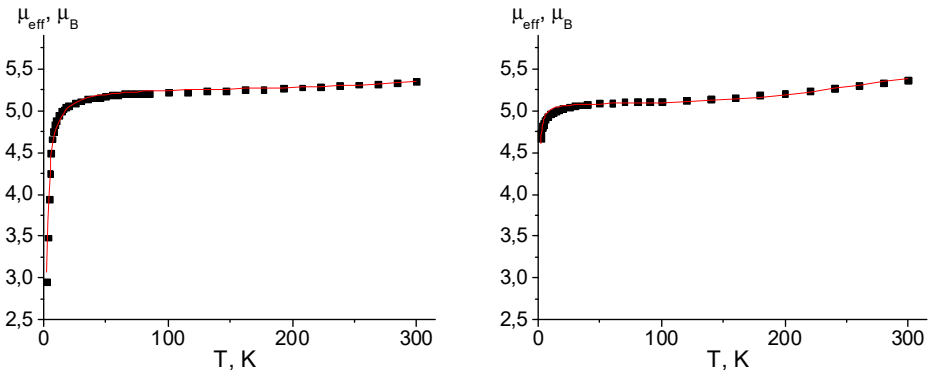

(**a**) (**b**)

Figure 7. The $\mu_{eff}(T)$ dependencies for complexes $[Mn(hfac)_2(NN\text{-}Pz\text{-}CH_2CH_2F)]_n$ (**a**) and $[Mn(hfac)_2(NN\text{-}Pz\text{-}CH_2CHF_2)]_n$ (**b**). Solid curves are theoretical ones.

Preprints (www.preprints.org) | NOT PEER-REVIEWED | Posted: 26 September 2023 doi:10.20944/preprints202309.1700.v1

For cyclic dimer [Mn(hfac)$_2$(NN-Pz-CH$_2$CF$_3$)]$_2$, the temperature dependence of μ_{eff} is presented in Figure 8a. The room temperature μ_{eff} value is approximately 7.52 μ_B. As the temperature is lowered, μ_{eff} slightly decreases, reaching a plateau of 7.20 μ_B at 100 K and then drops rapidly at temperatures below 15 K. In the temperature range of plateau 30–100 K, the observed μ_{eff} values are considerably less than the theoretical spin-only value (8.72 μ_B) for the non-interacting spin system of two Mn^{2+} ions and two nitroxide ligands based on the unit with the [Mn(hfac)$_2$(NN-Pz-CH$_2$CF$_3$)]$_2$ formula. As in the previous complexes, the observed magnetic behaviour of [Mn(hfac)$_2$(NN-Pz-CH$_2$CF$_3$)]$_2$ can be explained by the strong antiferromagnetic interactions in {Mn^{2+}–O˙⁻N<} exchange clusters, in which the spins of the coordinated N˙⁻O groups are completely coupled to the two spins of Mn^{2+}. Therefore, the magnetic susceptibility has contributions only from the residual moments of two exchange clusters (S = 2) (the theoretical spin-only magnetic moment of μ_{teor} = 6.93 μ_B). The further decrease in μ_{eff} at T < 10 can be attributed to the weak interactions between two-spin {Mn^{2+}–O˙⁻N<} exchange clusters. Analysis of the experimental $\mu_{eff}(T)$ dependences with a tetramer model using spin-Hamiltonian $H = -2J_1(S_{Mn1}S_{R1} + S_{Mn2}S_{R2}) - 2J_2(S_{Mn1}S_{R2} + S_{Mn2}S_{R1})$ as reported in refs. [58,62] gives the best fit values of g-factors and exchange interaction parameters J_1 and J_2: 2.0036 ± 0.002, –87.4 ± 1.3 cm^{-1} and 0.81 ± 0.01 cm^{-1}, respectively. Parameter J_1 corresponds to strong antiferromagnetic exchange in the {Mn^{2+}–O˙⁻N<} moieties, and J_2 corresponds to weak interactions between spins of the Mn^{2+} ion and the nitroxide coordinated via the N atom.

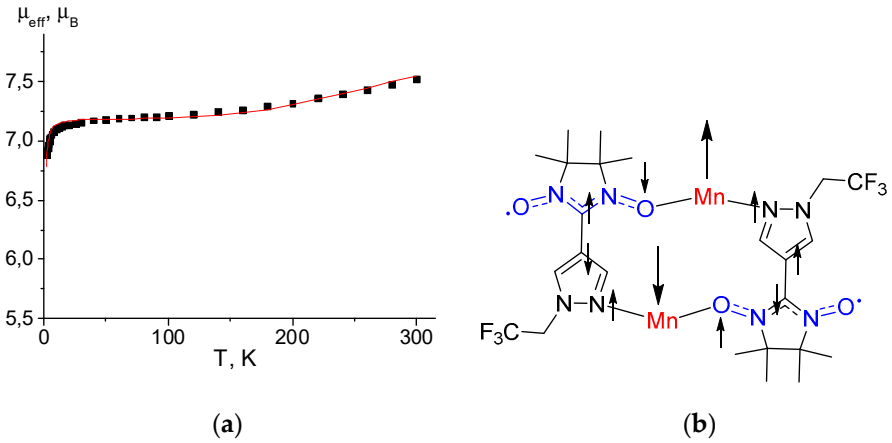

Figure 8. (**a**) The $\mu_{eff}(T)$ dependencies for complex [Mn(hfac)$_2$(NN-Pz-CH$_2$CF$_3$)]$_2$. The solid curve corresponds to the best theoretical fit. (**b**) The spin polarisation mechanism for the intra-dimer magnetic coupling.

The strong antiferromagnetic interaction can be attributed to the effective overlap between the π-SOMO orbital containing the unpaired electrons of the nitronyl nitroxide moiety and *d* orbitals of the Mn(II) ion [63]. The experimental J_1 value in [Mn(hfac)$_2$(NN-Pz-CH$_2$CF$_3$)]$_2$ has the same order of magnitude as that observed in different dimeric complexes (Table S2). The observed difference in antiferromagnetic coupling (from –74 to –208 cm^{-1}) may be ascribed to the different coordination geometry of the manganese–nitroxide spin cluster affecting the overlap of the magnetic orbitals. The small positive J_2 value shows that a weak ferromagnetic coupling exists between the two {Mn–O-N} moieties and is mediated by the pyrazole rings (Figure 8b) thus giving rise to the non-magnetic ground spin state. This weak ferromagnetic interaction can be explained by the spin polarization mechanism.

4. Conclusions

In summary, the complexation reaction of [Mn(hfac)$_2$] with pyrazolyl-substituted nitronyl nitroxides bearing various fluorinated alkyl groups (–CHF$_2$, –CH$_2$CH$_2$F, –CH$_2$CHF$_2$ or –CH$_2$CF$_3$) in the pyrazole core was investigated. The most interesting result of this investigation is that depending on the structure of the fluorinated alkyl substituent, the complexation reaction of [Mn(hfac)$_2$] with these radicals under identical conditions affords complexes of head-to-head chain-polymeric

structure, head-to-tail chain-polymeric structure or molecular structure. In all complexes, nitronyl nitroxide ligands act as a bridging ligand linking Mn(II) ions through the O atom of the nitroxide group and the N atom of the pyrazole ring, thereby creating three-spin {>N·–O–Mn^{2+}–O·–N<} or two-spin {Mn^{2+}–O·–N<} exchange clusters. According to magnetic measurements, in all the clusters, the Mn^{2+} ion strongly interacts antiferromagnetically with the coordinated nitroxide group. Our investigation shows that the structure of the metal–nitroxide complexes can be modulated by the step-by-step fluorination of the radical ligand thus making it possible to obtain coordination compounds with a previously unknown motif. Further studies on magnetostructural correlations of related organic and inorganic composite systems are in progress.

Supplementary Materials: The following supporting information can be downloaded at the website of this paper posted on Preprints.org, Figure S1: ORTEP drawings of a fragment of structure in co–crystal $[Mn(hfac)_2(NN–Pz–CH_2CHF_2)]_n$·n$[Mn(hfac)_2(NN–Pz–CH_2CHF_2)H_2O]$; Figure S2: The packing diagram for $[Mn(hfac)_2(NN–Pz–CH_2CF_3)]_2$·$2C_7H_8$; Figure S3: Experimental and calculated powder X-ray diffraction pattern of $[Mn(hfac)_2(NN\text{-}Pz\text{-}CHF_2)]_n$; Figure S4: Experimental and calculated powder X-ray diffraction pattern of $[Mn(hfac)_2(NN\text{-}Pz\text{-}CH_2CH_2F)]_n$; Figure S5: Experimental and calculated powder X-ray diffraction pattern of $[Mn(hfac)_2(NN\text{-}Pz\text{-}CH_2CHF_2)]_n$·$nC_7H_8$; Figure S6: Experimental and calculated powder X-ray diffraction pattern of $[Mn(hfac)_2(NN\text{-}Pz\text{-}CH_2CHF_2)]_n$; Figure S7: Experimental and calculated powder X-ray diffraction pattern of $[Mn(hfac)_2(NN\text{-}Pz\text{-}CH_2CF_3)]_2$·$2C_7H_8$. Table S1: Selected geometric parameters and experimental J_1 values in the $[Mn(hfac)_2(NN–Pz–CH_2CF_3)]_2$ dimer and cousin dimeric complexes of $Mn(hfac)_2$ with nitronyl nitroxides; Table S2: Selected bond distances in $[Mn(hfac)_2(NN–Pz–CHF_2)]_n$; Table S3: Selected bond distances in $[Mn(hfac)_2(NN–Pz–CH_2CH_2F)]_n$; Table S4: Selected bond distances in $[Mn(hfac)_2(NN–Pz–CH_2CHF_2)]_n$; Table S5: Selected bond distances in $[Mn(hfac)_2(NN–Pz–CH_2CHF_2)]_n$·$nC_7H_8$; Table S6: Selected bond distances in $[Mn(hfac)_2(NN–Pz–CH_2CF_3)]_2$·$2C_7H_8$; Tables S7 and S8: XRD data on the manganese–nitroxide complexes. References [64–66] are cited in the Supplementary Materials.

Author Contributions: Conceptualization, E.T.; methodology, B.U. and N.E.; validation, N.E. and A.B.; formal analysis, A.K. and A.B.; investigation, E.K., A.S., B.U, T.D., D.N., A.K., M.Z., N.E. and A.B.; writing—original draft preparation, E.T.; writing—review and editing, E.T.; supervision, N.E. and E.T.; project administration, E.T. All authors have read and agreed to the published version of the manuscript.

Funding: The authors thank the Russian Science Foundation for funding (project No. 21-73-20079).

Data Availability Statement: The data that support the findings of this study are available upon reasonable request from the authors.

Acknowledgments: The crystal structures of $[Mn(hfac)_2(NN\text{-}Pz\text{-}CHF_2)]_n$, $[Mn(hfac)_2(NN\text{-}Pz\text{-}CH_2CH_2F)]_n$, $[Mn(hfac)_2(NN\text{-}Pz\text{-}CH_2CHF_2)]_n$·$nC_7H_8$ and $[Mn(hfac)_2(NN\text{-}Pz\text{-}CH_2CF_3)]_2$·$C_7H_8$ were solved in the Department of Structural Studies at N. D. Zelinsky Institute of Organic Chemistry, Moscow. The crystal structure of the $[Mn(hfac)_2(NN\text{-}Pz\text{-}CH_2CHF_2)]_n$ complex was solved at the Center for Molecular Composition Studies at INEOS RAS (contract No. 075-03-2023-642 with the Ministry of Science and Higher Education of the Russian Federation).

Conflicts of Interest: The authors declare no conflict of interest.

References

1. Benelli, C.; Gatteschi, D. Magnetism of Lanthanides in Molecular Materials with Transition-Metal Ions and Organic Radicals. *Chem. Rev.* **2002**, *102*, 2369–2388.
2. Tretyakov, E. V.; Ovcharenko, V. I.; Terent'ev, A. O.; Krylov, I. B.; Magdesieva, T. V.; Mazhukin, D. G.; Gritsan, N. P. Conjugated nitroxides. *Russ. Chem. Rev.* **2022**, *91*, RCR5025.
3. Ovcharenko, V. Metal-Nitroxide Complexes: Synthesis and Magnetostructural Correlations. In *Stable Radicals*; Hicks, R. G., Ed.; John Wiley & Sons, Ltd: Chichester, UK, 2010; pp 461−506.
4. Ferrando-Soria, J.; Vallejo, J.; Castellano, M.; Martínez-Lillo, J.; Pardo, E.; Cano, J.; Castro, I.; Lloret, F.; Ruiz-García, R.; Julve, M. Molecular magnetism, quo vadis? A historical perspective from a coordination chemist viewpoint. *Coord. Chem. Rev.* **2017**, *339*, 17–103.
5. Bernot, K.; Pointillart, F.; Rosa, P.; Etienne, M.; Sessoli, R;. Gattesch, D. Single molecule magnet behaviour in robust dysprosium–biradical complexes. *Chem. Commun.* **2010**, *35*, 6458–6460.
6. Wang, J.; Miao, H.; Xiao, Z. X.; Zhou, Y.; Deng, L.;D.; Zhang, Y. Q.; Wang, X. Y. Syntheses, structures and magnetic properties of the lanthanide complexes of the pyrimidyl-substituted nitronyl nitroxide radical. *Dalton Trans.* **2017**, *31*, 10452–10461.
7. Kadilenko, E. M.; Gritsan, N. P.; Tretyakov, E. V.; Fokin, S. V.; Romanenko, G. V.; Bogomyakov, A. S.; Gorbunov, D. E.; Schollmeyer, D.; Baumgarten, M.; Ovcharenko, V. I. A black-box approach to the

construction of metal-radical multispin systems and analysis of their magnetic properties. *Dalton Trans.* **2020**, *49*, 16916–6927.
8. Sun, J.; Xi, L.; Xie, J.; Wang, K.; Li, L. C.; Sutter, J. P. A loop chain and a three-dimensional network assembled from a multi-dentate nitronyl nitroxide radical and $M(hfac)_2$ (M = CoII, CuII). *Dalton Trans.* **2018**, *47*, 14630–14635.
9. Li, H. D.; Sun, J.; Yang, M.; Sun, Z.; Xie, J.; Ma, Y.; Li, L. C. Functionalized nitronyl nitroxide biradical bridged one-dimensional lanthanide chains: slow magnetic relaxation in the Tb and Dy analogues. *New J. Chem.* **2017**, *41*, 10181–10188.
10. Haraguchi, M.; Tretyakov, E.; Gritsan, N.; Romanenko, G.; Gorbunov, D.; Bogomyakov, A.; Maryunina, K.; Suzuki, S.; Kozaki, M.; Shiomi, D.; Sato, K.; Takui, T.; Nishihara, S.; Inoue, K.; Okada, K. (Azulene-1,3-diyl)-bis(nitronyl nitroxide) and (Azulene-1,3-diyl)-bis(iminonitroxide) and Their Copper Complexes. *Chem Asian J.* **2017**, *12*, 2929–2941.
11. Barskaya, I. Yu.; Veber, S. L.; Suturina, E. A.; Sherin, P. S.; Maryunina, K. Yu.; Artiukhova, N. A.; Tretyakov, E. V.; Sagdeev, R. Z.; Ovcharenko, V. I.; Gritsan, N. P.; Fedin. M. V. Spin-state-correlated optical properties of copper(II)–nitroxide based molecular magnets. *Dalton Trans.* **2017**, *46*, 13108–13117.
12. Kaszub, W.; Marino, A.; Lorenc, M.; Collet, E.; Bagryanskaya, E. G.; Tretyakov, E. V.; Ovcharenko, V. I.; Fedin, M. V. Ultrafast Photoswitching in a Copper-Nitroxide-Based Molecular Magnet. *Angew. Chem., Intern. Ed.* **2014**, *53*, 10636–10640.
13. Rinehart, J. D.; Fang, M.; Evans, W. J.; Long, J. R. A N_2^{3-} Radical-Bridged Terbium Complex Exhibiting Magnetic Hysteresis at 14 K. *J. Am. Chem. Soc.* **2011**, *133*, 14236–14239.
14. Rinehart, J. D.; Fang, M.; Evans, W. J.; Long, J. R. Strong exchange and magnetic blocking in N_2^{3-}-radical-bridged lanthanide complexes. *Nat. Chem.* **2011**, *3*, 538–542.
15. Novitchi, G.; Shova, S.; Train, C. Investigation by Chemical Substitution within 2p-3d-4f Clusters of the Cobalt(II) Role in the Magnetic Behavior of $[vdCoLn]_2$ (vd = Verdazyl Radical). *Inorg. Chem.* **2022**, *61*, 17037–17048.
16. Ishii, N.; Okamura, Y.; Chiba, S.; Nogami, T.; Ishida. T. Giant coercivity in a one-dimensional cobalt-radical coordination magnet. *J. Am. Chem. Soc.* **2008**, *130*, 24–25.
17. Maria, G. F. V.; Cassaro, R. A. A.; Akpinar, H.; Schlueter, J. A.; Lahti, P. M.; Novak, M. A. A Cobalt Pyrenylnitronylnitroxide Single-Chain Magnet with High Coercivity and Record Blocking Temperature. *Chem. Eur. J.* **2014**, *20*, 5460–5467.
18. Barskaya, I. Yu.; Veber, S. L.; Fokin, S. V.; Tretyakov, E. V.; Bagryanskaya, E. G.; Ovcharenko, V. I.; Fedin, M. V. Structural specifics of light-induced metastable states in copper(II)–nitroxide molecular magnets. *Dalton Trans.* **2015**, *44*, 20883–20888.
19. Tretyakov, E. V.; Romanenko, G. V.; Veber, S. L.; Fedin, M. V.; Polushkin, A. V.; Tkacheva, A. O.; Ovcharenko, V. I. $Cu(hfac)_2$ Complexes with Nitronyl Ketones Structurally Mimicking Nitronyl Nitroxides in Breathing Crystals. *Aust. J. Chem.* **2015**, *68*, 970–980.
20. Furui, T.; Suzuki, S.; Kozaki, M.; Shiomi, D.; Sato, K.; Takui, T.; Okada, K.; Tretyakov, E. V.; Tolstikov, S. E.; Romanenko, G. V.; Ovcharenko, V. I. Preparation and Magnetic Properties of Metal-Complexes from N-t-Butyl-N-oxidanyl-2-amino-(nitronyl nitroxide). Inorg. Chem. 2014, 53, 802–809.
21. Tretyakov, E. V.; Fedyushin, P. A.; Panteleeva, E. V.; Stass, D. V.; Bagryanskaya, I. Yu.; Beregovaya, I. V.; Bogomyakov, A. S. Substitution of a Fluorine Atom in Perfluorobenzonitrile by a Lithiated Nitronyl Nitroxide. *J. Org. Chem.* **2017**, *82*, 4179–4185.
22. Tretyakov, E.; Fedyushin, P.; Panteleeva, E.; Gurskaya, L.; Rybalova, T.; Bogomyakov, A.; Zaytseva, E.; Kazantsev, M.; Shundrina, I.; Ovcharenko, V. Aromatic SNF-Approach to Fluorinated Phenyl *tert*-Butyl Nitroxides. *Molecules* **2019**, *24*, 4493.
23. Politanskaya, L. V.; Fedyushin, P. A.; Rybalova, T. V.; Bogomyakov, A. S.; Asanbaeva, N. B.; Tretyakov, E. V. Fluorinated Organic Paramagnetic Building Blocks for Cross-Coupling Reactions. *Molecules* **2020**, *25*, 5427.
24. Fedyushin, P.; Rybalova, T.; Asanbaeva, N.; Bagryanskaya, E.; Dmitriev, A.; Gritsan, N.; Kazantsev, M.; Tretyakov, E. Synthesis of Nitroxide Diradical Using a New Approach. *Molecules* **2020**, *25*, 2701.
25. Serykh, A.; Tretyakov, E.; Fedyushin, P.; Ugrak, B.; Dutova, T.; Lalov, A.; Korlyukov, A.; Akyeva, A.; Syroeshkin, M.; Bogomyakov, A.; Romanenko, G.; Artiukhova, N.; Egorov, M., Ovcharenko, V. *N*-Fluoroalkylpyrazolyl-substituted Nitronyl Nitroxides. *J. Mol. Struct.* **2022**, *1269*, 133739.
26. Tretyakov, E. V.; Fedyushin, P. A. Polyfluorinated organic paramagnets. *Russ. Chem. Bull.* **2021**, *70*, 2298–2314.
27. Zayakin, I. A.; Korlyukov, A. A.; Gorbunov, D. E.; Gritsan, N. P.; Akyeva, A. Ya.; Syroeshkin, M. A.; Stass, D. V.; Tretyakov, E. V.; Egorov, M. P. Au–Au Chemical Bonding in Nitronyl Nitroxide Gold(I) Derivatives. *Organometallics* **2022**, *41*, 1710–1720.
28. Tretyakov, E.; Fedyushin, P.; Bakuleva, N.; Korlyukov, A.; Dorovatovskii, P.; Gritsan, N.; Dmitriev, A.; Akyeva, A.; Syroeshkin, M.; Stass, D.; Zykin, M.; Efimov, N.; Luneau, D. Series of Fluorinated

Benzimidazole-Substituted Nitronyl Nitroxides: Synthesis, Structure, Acidity, Redox Properties, and Magnetostructural Correlations. *J. Org. Chem.* **2023**, *88*, 10355–10370.
29. Reichenbächer, K.; Su¨ss, H. I.; Hulliger, J. Fluorine in crystal engineering—"the little atom that could". *Chem. Soc. Rev.* **2005**, *34*, 22–30.
30. Schwarzer, A.; Weber, E. Influence of Fluorine Substitution on the Crystal Packing of N-Phenylmaleimides and Corresponding Phthalimides. *Cryst. Growth Des.* **2008**, *8*, 2862–2874.
31. Singla, L.; Yadav, H. R.; Choudhury, A. R. Structural and Computational Analysis of Organic Fluorine-Mediated Interactions in Controlling the Crystal Packing of Tetrafluorinated Secondary Amides in the Presence of Weak C–H···O=C Hydrogen Bonds. *Cryst. Growth Des.* **2022**, *22*, 1604–1622.
32. Levina, E. O.; Chernyshov, I. Y.; Voronin, A. P.; Alekseiko, L. N.; Stash, A. I.; Vener, M. V. Solving the enigma of weak fluorine contacts in the solid state: a periodic DFT study of fluorinated organic crystals. *RSC Adv.* **2019**, *9*, 12520–12537.
33. Hebeisen, P.; Weiss, U.; Alker, A.; Kuhn, B.; Müller, K.; Wang, F.; Prakash, G. K. S. Molecular Structure and Crystal Packing of Monofluoromethoxyarenes. *Eur. J. Org. Chem.* **2018**, 3724–3734.
34. Berger, R.; Resnati, G.; Metrangolo, P.; Weberd, E.; Hulliger, J. Organic fluorine compounds: a great opportunity for enhanced materials properties. *Chem. Soc. Rev.* **2011**, *40*, 3496–3508.
35. Chopra, D.; Guru Row, T. N. Role of organic fluorine in crystal engineering. *CrystEngComm* **2011**, *13*, 2175–2186.
36. Cole, J. C.; Taylor, R. Intermolecular Interactions of Organic Fluorine Seen in Perspective. *Cryst. Growth Des.* **2022**, *22*, 1352–1364.
37. Dunitz, J. D. Organic Fluorine: Odd Man Out. *ChemBioChem.* **2004**, *5*, 614–621.
38. Murray, J. S.; Seybold, P. G.; Politzer, P. The Many Faces of Fluorine: Some Noncovalent Interactions of Fluorine Compounds. *J. Chem. Thermodyn.* **2021**, *156*, 106382.
39. Varadwaj, A.; Marques, H. M.; Varadwaj, P. R. Nature of Halogen-Centered Intermolecular Interactions in Crystal Growth and Design: Fluorine-Centered Interactions in Dimers in Crystalline Hexafluoropropylene as a Prototype. *J. Comput. Chem.* **2019**, *40*, 1836–1860.
40. CrysAlisPro. Version 1.171.41.106a. *Rigaku Oxford Diffraction*, 2021.
41. Sheldrick, G. M. SHELXT - Integrated space-group and crystal-structure determination. *Acta Crystallogr. A* **2015**, *71*, 3–8.
42. Sheldrick, G. M. Crystal structure refinement with SHELXL. *Acta Crystallogr. C* **2015**, *71*, 3–8.
43. Dolomanov, O. V.; Bourhis, L. J.; Gildea, R. J.; Howard, J. A. K.; Puschmann, H. OLEX2: a complete structure solution, refinement and analysis program. *J. Appl. Cryst.* **2009**, *42*, 229–341.
44. Bruker APEX3, RLATT, CELL_NOW, TWINABS, SAINT-Plus and SADABS. Bruker AXS Inc., Madison, Wisconsin, USA, 2016.
45. Carlin, R. L. *Magnetochemistry*. Springer Berlin, Germany, 1986.
46. Romanenko, G. V.; Fokin, S. V.; Vasilevskii, S. F.; Tretyakov, E. V.; Shvedenkov, Yu. G.; Ovcharenko, V. I. Dimeric Complexes of Manganese(II) and Nickel(II) Hexafluoroacetylacetonates with Pyrazole-Containing Nitronylnitroxyl Radicals. *Russ. J. Coord. Chem.* **2001**, *27*, 360–367.
47. Maryunina, K.; Fokin, S.; Ovcharenko, V.; Romanenko, G.; Ikorskii, V. Solid solutions: An efficient way to control the temperature of spin transition in heterospin crystals MxCu1 − x(hfac)2L (M = Mn, Ni, Co; L = nitronyl nitroxide). *Polyhedron* **2005**, *24*, 2094–2101.
48. Caneschi, A.; Gatteschi, D.; Sessoli, R. Magnetic properties of a layered molecular material comprising manganese hexafluoroacetylacetonate and nitronyl nitroxide radicals. *Inorg. Chem.* **1993**, *32*, 4612-4616.
49. Okada, K.; Nagao, O.; Mori, H.; Kozaki, M.; Shiomi, D.; Sato, K.; Takui, T.; Kitagawa, Y.; Yamaguchi, K. Preparation and Magnetic Properties of Mn(hfac)2-Complexes of 2-(5-Pyrimidinyl)- and 2-(3-Pyridyl)-Substituted Nitronyl Nitroxides. *Inorg. Chem.* **2003**, *42*, 3221–3228.
50. Zhu, M.; Lou, D.; Deng, X.; Zhang, L.; Zhang, W.; Lü, Y. A functional nitroxide ligand builds up two 2p–3d complexes with different spin ground states and a 2p–3d–4f chain of rings. *CrystEngComm* **2018**, *20*, 2583–2592.
51. Okada, K.; Beppu, S.; Tanaka, K.; Kuratsu, M.; Furuichi, K.; Kozaki, M.; Suzuki, S.; Shiomi, D.; Sato, K.; Takui, T.; Kitagawa, Y;. Yamaguchi, K. Preparation, structure, and magnetic interaction of a Mn(hfac)2-bridged [2-(3-pyridyl)(nitronyl nitroxide)–Mn(hfac)2]2 chain complex. *Chem. Commun.* **2007**, 2485–2487.
52. Field, L. M.; Lahti, P. M.; Palacio, F. 1:1 Complexes of 5-(4-[N-tert-butyl-N-aminoxyl]phenyl)pyrimidine with manganese(II) and copper(II) hexafluoroacetonylacetonate. *Chem. Commun.* **2002**, 636–637.
53. Wang, H.-M.; Liu, Z.-L.; Liu, C.-M.; Zhang, D.-Q.; Lu, Z.-L.; Geng, H.; Shuai, Z.-G.; Zhu, D.-B. Coordination Complexes of 2-(4-Quinolyl)nitronyl Nitroxide with M(hfac)2 [M = Mn(II), Co(II), and Cu(II)]: Syntheses, Crystal Structures, and Magnetic Characterization. *Inorg. Chem.* **2004**, *43*, 4091–4098.
54. Zhou, N.; Wang, Y.-L.; Wang, H.-L.; Li, W.-J.; Guo, Z.; Ma, Y.; Li, L.-C.; Wang, Q.-L.; Cheng, P.; Liao, D.-Z. Structural design and magnetic properties study on two nitronyl nitroxide radicals–MnII complexes with hetero chain or mononuclear tri-spin structures. *Polyhedron* **2015**, *89*, 96–100.

55. Liu, R.-N.; Li, L.-C.; Xing, X.-Y.; Liao, D.-Z. Cyclic metal–radical complexes based on 2-[4-(1-imidazole)phenyl]-4,4,5,5-tetramethylimidazoline-1-oxyl-3-oxide: Syntheses, crystal structures and magnetic properties. *Inorganica Chim. Acta* **2009**, *362*, 2253–2258.
56. Fokin, S. V.; Tolstikov, S. E.; Tret'yakov, E. V.; Romanenko, G. V.; Bogomyakov, A. S.; Veber, S. L.; Sagdeev, R. Z.; Ovcharenko, V. I. Molecular magnets based on chain polymer complexes of copper(II) bis(hexafluoroacetylacetonate) with isoxazolylsubstituted nitronyl nitroxides. *Russ. Chem. Bull.* **2011**, *60*, 2470–2484.
57. Yang, M.; Xie, S.; Liang, X.; Zhang, Y.; Dong, W. A novel functional nitronyl nitroxide and its manganese and cobalt complexes: Synthesis, structures and magnetic properties. *Polyhedron* **2019**, *161*, 132–136.
58. Wang, C.; Ma, Y.; Wang, Y.; Wang, Q.; Li, L.; Cheng, P.; Liao, D. A New Quinoxalinyl-Substituted Nitronyl Nitroxide Radical and its Five-Spin CuII and Four-Spin MnII Complexes: Syntheses, Crystal Structures, and Magnetic Properties. *Aust. J. Chem.* **2012**, *65*, 672–679.
59. Mei, Z.; Dingshuo, L.; Xiaochun, D.; Li, Z.; Wei, Z.; Yaohong, L. A functional nitroxide ligand builds up two 2p–3d complexes with different spin ground states and a 2p–3d–4f chain of rings. *CrystEngComm* **2018**, *20*, 2583–2592.
60. Maryunina, K.; Fokin, S.; Ovcharenko, V.; Romanenko, G.; Ikorskii, V. Solid solutions: An efficient way to control the temperature of spin transition in heterospin crystals $M_xCu_{1-x}(hfac)_2L$ (M = Mn, Ni, Co; L = nitronyl nitroxide). *Polyhedron* **2005**, *24*, 2094–2101.
61. Zhang, J.-Y.; Liu, C.-M.; Zhang, D.-Q.; Gao, S.; Zhu, D.-B. Syntheses, crystal structures, and magnetic properties of two cyclic dimer M_2L_2 complexes constructed from a new nitronyl nitroxide ligand and $M(hfac)_2$ ($M = Cu^{2+}$, Mn^{2+}). *Inorganica Chim. Acta* **2007**, *360*, 3553–3559.
62. Borra´s-Almenar, J. J.; Clemente-Juan, J. M.; Coronado, E.; Tsukerblat, B. S. MAGPACK[1] A package to calculate the energy levels, bulk magnetic properties, and inelastic neutron scattering spectra of high nuclearity spin clusters. *J. Comput. Chem.* **2001**, *22*, 985–991.
63. Caneschi, A.; Gatteschi, D.; Sessoli, R.; Rey, P. Toward molecular magnets: the metal-radical approach. *Acc. Chem. Res.* **1989**, *22*, 392–398.
64. Caneschi, A.; Gatteschi, D.; Sessoli, R.; Rey, P. Structure and magnetic properties of a ring of four spins formed by manganese(II) and a pyridine substituted nitronyl nitroxide. *Inorganica Chim. Acta* **1991**, *184*, 67–71.
65. Guo, J.-N.; Wang, J.-J.; Sun, G.-F.; Li, H.-D.; Li, L.-C. A novel nitronyl nitroxide radical containing thiophene and pyridine rings and its manganese(II) complex: synthesis, structure, and magnetic properties. *J. Coord. Chem.* **2017**, *70*, 1926–1935.
66. Rancurel, C.; Leznoff, D. B.; Sutter, J.-P.; Golhen, S.; Ouahab, L.; Kliava, J.; Kahn, O. Synthesis, Structure, and Magnetism of Mono- and Binuclear Manganese(II) Compounds of Nitronyl Nitroxide Substituted Phosphine Oxides. *Inorg. Chem.* **1999**, *38*, 4753−47538.